OPEN ACCESS

University of BRISTOL

Peer reviewed version

License (if available):
CC BY-NC

Link to published version (if available):
10.1021/jacs.6b00537

Link to publication record in Explore Bristol Research
PDF-document

University of Bristol - Explore Bristol Research
General rights

Spin state as a probe of vesicle self-assembly

Sanghoon Kim,[a] Christine Bellouard,*[b] Julian Eastoe,[c] Nadia Canilho,[a] Sarah E Rogers,[d] Dris Ihiawakrim,[e] Ovidiu Ersen[e] and Andreea Pasc*[a]

[a] SRSMC, UMR 7565, Université de Lorraine/CNRS, F-54506 Vandoeuvre-lès-Nancy, France ; [b]Institut Jean Lamour, UMR 7198, Université de Lorraine/CNRS, F-54506 Vandoeuvre-lès-Nancy, France ; [c]School of Chemistry, University of Bristol, Cantock's Close, Bristol, BS8 1TS, UK; [d] Rutherford Appleton Laboratory, ISIS Facility, Chilton, Oxfordshire OX11 0QX, UK; [e]Institut de Physique et Chimie des Matériaux de Strasbourg, UMR7504 CNRS - Université de Strasbourg, 23 rue du Loess, BP 43, 67034 Strasbourg cedex 2, France.

Supporting Information Placeholder

ABSTRACT: A novel system of paramagnetic vesicles was designed using ion pairs of iron-containing surfactants. Unilamellar vesicles (diameter ~200 nm) formed spontaneously and were characterized by cryogenic transmission electron microscopy, nanoparticle tracking analysis, light and small-angle neutron scattering. Moreover, for the first time, it is shown that magnetization measurements can be used to investigate self-assembly of such functionalized systems, giving information on the vesicle compositions and distribution of surfactants between the bilayers and the aqueous bulk.

In recent years, vesicles have been widely studied for potential applications in diverse fields such as biomedicine,[1-4] catalysis[5-7] and cosmetics.[8] Vesicles are spherical self-assembly systems comprising lipid bilayer membranes enclosing internal aqueous compartments. Since vesicles are structurally similar to biological membranes, they are considered as cell mimics.[9] Furthermore, vesicles are employed to encapsulate fragrances, flavors or drugs for controlled release. Functional vesicles which respond to external stimuli such as temperature,[10] pH,[11,12] redox[13,14] and magnetic field gradient,[15-17] have been widely studied as drug nanovectors. In terms of triggerable systems, magnetic vesicles are of significant interest because magnetic properties can be beneficial in applications like magnetic resonance imaging (MRI) or hyperthermia as well as spatial and temporal drug targeting.[18-21]

To generate magnetic vesicles three approaches have been used to date: firstly, loading magnetic nanoparticles in the internal aqueous core [16,20-23]; embedding nanoparticles within the hydrophobic tails of the lipids of the bilayers.[24-25] and finally, encapsulating nanoparticles between bilayers of multilamellar membranes.[26,27]

An alternative strategy is employed here, by introducing magnetic surfactants or lipids in the bilayers.

Recently, magneto-responsive surfactants (MagSurfs)[28] have been introduced opening up a range of interesting magnetic colloidal systems such as micelles,[29] emulsions,[30] solid lipid nanoparticles,[31] organosols[32] or magnetized DNA.[33] These MagSurfs have also been used as structure directing agents for synthesis of magnetic mesoporous silica materials.[34] Here is reported, for the first time, new paramagnetic vesicles which can be readily generated from ion pairs of anionic and cationic iron-surfactants. This strategy was inspired from the well-known catanionic surfactants[35-37] that are able to spontaneously form vesicles in a range of anion/cation ratio (r) close to stoichiometry. Herein, exploiting the paramagnetic properties of Fe^{3+}, it is possible to investigate more accurately the range of self-assembly of surfactant ion pairs into vesicles and to give a clear picture of the partitioning between vesicles and bulk.

The necessary Fe^{3+} MagSurfs can be prepared from conventional surfactants, cationic dodecyltrimethylammonium bromide (DTAB) and anionic sodium bis(2-ethylhexyl) sulfosuccinate (AOT) to afford DTAF and AOT_3F respectively.
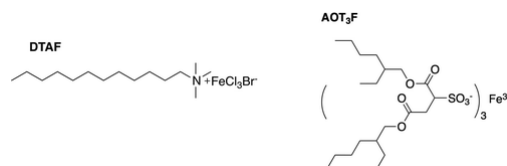
Scheme 1: Molecular structures of MagSurfs (AOT_3F and DTAF)

The behavior of these MagSurfs (AOT_3F, DTAF) in aqueous solutions is close to those of the parent surfactants. The single chain DTAF has a critical micelle concentration (CMC) of 13.6 mM at 25°C, which is similar to that of DTAB (15.5 mM).[28] However, its melting point decreases from 246°C to 32°C. The critical micelle concentration of AOT_3F is 2.2 mM (with respect to AOT moiety, or 0.73 mM with respect to AOT_3F), which is also close to CMC of the parent surfactant, AOT (~2.5 mM).[38]

Two series of four solutions denoted Ax and Bx, (with x= 1, 2, 3 ,4) have been prepared. A and B stand for two different surfactant concentration ratio r= C_{DATF} / C_{AOT3F}: 3.7 and 8.1 respectively. Those ratios were chosen in order to investigate both the self-assembly near stoichiometry between ionic pairs (3.7) and far from stoichiometry, in a domain rather rich in

DTAF. The total surfactant concentrations of A1 and B1 are respectively 21.4 mM and 15.2 mM. Then, these solutions have been two-fold diluted from Ax-1 (Bx-1) to Ax (Bx), x>1 is then the number of two-fold dilution of A1 (B1).

Gentle mixing of both surfactants spontaneously results in vesicles, as shown in Figures 1 (a) and (b) by cryogenic transmission electron microscopy (TEM), and in Figures 1 (c) and (d) by scanning transmission electron microscopy (STEM). Cryo-TEM is the typical powerful method to characterize soft matter, in similar conditions as magnetic measurements, and to avoid artifacts that might occur by drying. Moreover, recently, also Cryo-STEM appears as an imaging mode perfectly adapted to the direct observation of colloids, cells or vesicles in water media. For both series, the visualized vesicles have sizes of about 200 nm. However, smaller vesicles of about 100 nm were also observed (figure 1(b),1(c) and S1). It should be noted that these vesicles are out-of-equilibrium systems and therefore the systems is not perfectly monodisperse. In addition to TEM, scanning TEM allow to gather further insights into the surface morphology of the particles. For example, in Figure 1(d) we observe (up) a top view of a vesicle showing an almost identical phase contrast and (down) an inside view in the vesicle allowing us to see its hollow structure.
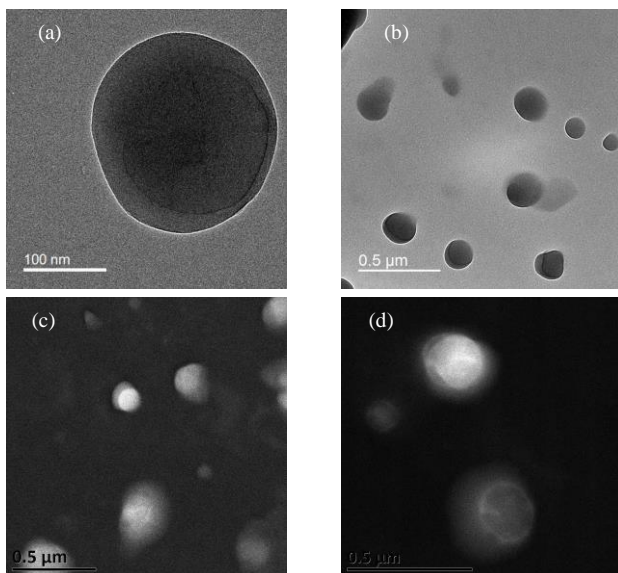

Figure 1: Cryo-TEM images of vesicles observed for A2 (a), A3 (b); Cryo-STEM images of vesicles observed for A2 (c), B2 (d).
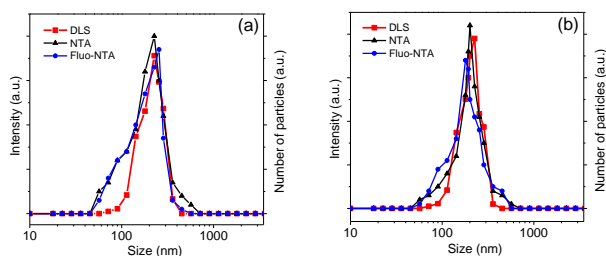

Figure 2. Size distribution of MagSurf vesicles measured for A1 (a) and B1 (b), using DLS (red, ■), NTA (black, ▲), and NTA with fluorescence filter blue, ●).

Dynamic light scattering (DLS) measurements and nanoparticle tracking analysis (NTA) allow to further characterize the size distribution (Figure 2). For both series (A1 and B1), DLS size distribution is centered at about 200 nm. Moreover, as shown in Figure S2, the size distribution do not depend on the composition ratio r. The size distribution observed by NTA exhibit a shoulder for smaller sizes (around roughly 100 nm) which are also present in TEM and STEM images, but are not seen by DLS. As DLS is a scattering technique providing an intensity proportional to the number of particles weighted by the square of the volume and NTA gives directly a number value of particles, smallest particles appears in NTA but not in DLS, where bigger particle sizes are screening the smaller one. Moreover, the use of a fluorescence filter with NTA allows detection of fluorescent aggregates containing iron ions (Video in SI). This is direct proof that the iron counterions are in the vesicle hydration shells.

The structures of these magnetic vesicles were also investigated using small-angle neutron scattering (SANS). Vesicle samples were prepared in D_2O in order to enhance the neutron scattering contrast. Shown in Figure 3(a) and (b) are SANS intensities I(q) for the Ax and Bx series as a function of scattering vector q, the curves have been normalized with respect to the total surfactant concentration C_T (Table S1). For the A1 to 3 and B1 to 2 samples, the low q regions exhibit clear q^{-2} decays, which is a general feature of SANS from locally planar surface structures, such as bilayers or vesicles.[39] In addition, the normalized SANS data for A1 to 3 (Figure 3(a)) and B1 to 2 (Figure 3(b)) show a common q dependence; indicating that the vesicles have similar, concentration-independent structures. The SANS data were fitted using a non-interacting polydisperse vesicle form factor model (Sasview[40] HardsphereStructure for P(Q)*S(Q)). The I(q) profiles from all samples A1 to 3, B1 to 2 are well described by this model, as illustrated in Figure 3(c) for A1 and B1. The shell thicknesses τ were approximately 2.5 nm (Table S1). The fitted values for τ suggest the vesicles are unilamellar, since 2.5 nm corresponds about $2 \times C_{12}$ disordered alkyl chain lengths. All parameters deduced from DLS and SANS are very similar for the A and B series (Table S1), moreover, the concentration-normalized I(q) superimposes as a function of AOT concentration (Figure 3(d)). This shows that the vesicles are not affected by the ratio r, and that vesicle concentration is proportional to AOT_3F concentration for both r ratios. The abrupt change in I(q) observed between A3 and A4 (figure 3(a)) and between B2 and B3 (figure 3(b)) indicates a transition from vesicles towards less well-defined aggregates on dilution. The critical vesicle concentrations (CVCs) can be estimated from these dilution series of I(q): CVC is between 5.4 mM and 2.7 mM (1.13 and 0.56 mM AOT_3F) for the DTAF/ AOT_3F ratio r of 3.7 and between 7.6 mM and 3.8 mM (0.84 and 0.42mM AOT_3F) for DTAF/ AOT_3F for r = 8.1.

On the other hand, the critical aggregation concentration (CAC) was estimated using surface tension measurements (Fig S3). The CAC value, expressed as a function of AOT_3F concentration, is essentially identical for both DTAF/AOT_3F ratios: about 1.5×10^{-2} mM which corresponds to a total surfactant concentration of 7.10^{-2}mM for r =3.7; and about 0.13 mM for r =8.1.

All these results suggest that the self-assembly mechanism of AOT_3F and DTAF ion pairs with increasing concentration in aqueous solution involves a transition from primary mixed aggregates to vesicles. This behavior was already observed for

catanionic surfactants that also undergo vesicle formation.[41,42] However, to date no clear evidence of the composition of the vesicle bilayers as well as on the distribution of the surfactants between the bilayers and the bulk has been presented. This is done here, by taking advantage of the paramagnetic properties of these MagSurfs: magnetic measurements were performed at low temperature.

Figure 3(a) and (b) present the temperature dependence of magnetization measured in an applied field of 70 kOe for the A and B series respectively. Interestingly, these curves exhibit qualitative behavior which correlates with the SANS data (Figures 2(a) and (b)): magnetization of A1-3 and B1-2 reported per Fe weight are almost superimposed as were SANS data, whereas a notable decrease is clearly observed on further dilution, from A3 to A4, and B2 to B3, as the vesicles are disrupted. Moreover, the measured magnetization at low temperature of A1-3 (≈ 420 emu/g) is quite close to the saturation magnetization of Fe^{3+} ions with S=5/2 ($M_s^{5/2} = 500$ emu/g_{Fe}) whereas it is much lower for B1-2 (≈ 300 emu/g), which has a lower vesicle concentration. The decrease in signal observed after vesicle breakup (from A3 to A4, or B2 to B3) or with decreasing vesicle concentration (from A1-3 to B1-2) is attributed to a Fe^{3+} spin crossover from high spin (5/2) to low spin state (1/2).
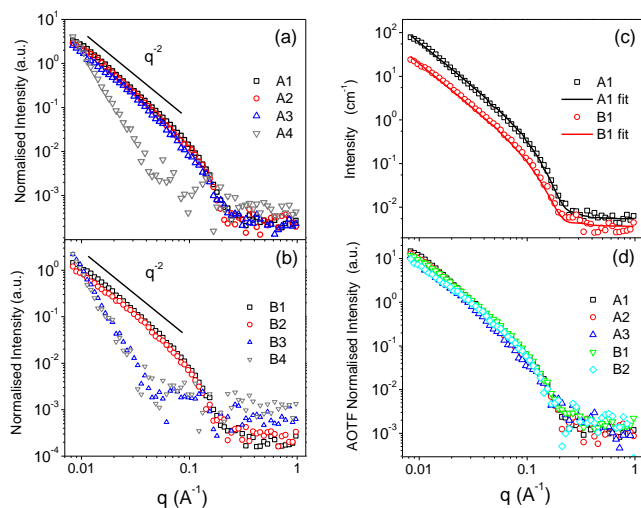

Figure 3. Small-angle neutron scattering data normalized to total molar MagSurf concentration for Ax (a), Bx (b), fitted data for A1 and B1 (c), normalized SANS data with respect to AOT$_3$F concentration for A1-3 and B1-2.
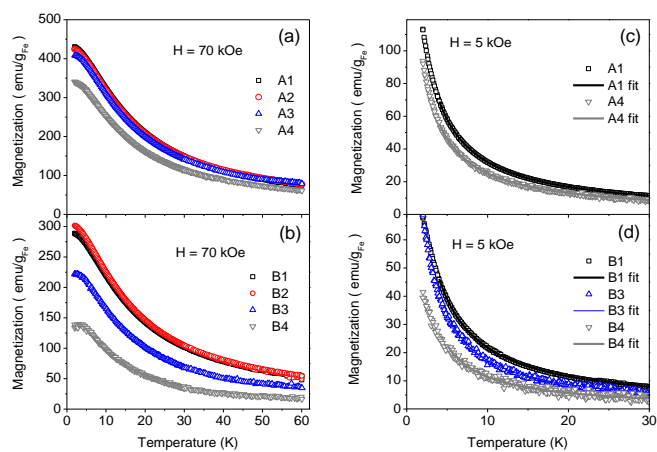

Figure 4. Magnetization measurements as a function of temperature at 70 kOe for A1-4 (a), B1-4 (b), at 5 kOe for A1&4 (c) ; B1&3-4 (d). The lines in figures (c) and (d) are fits with a sum of two Brillouin functions as described in the text.

To obtain the fraction of high spins with respect to low spins, the low field (H= 5 kOe) temperature magnetization has been fitted with the contribution of two Brillouin functions as described in supplementary information. The lines in Figure 3(c) and (d) correspond to the sum of the Brillouin functions with fitted parameters. The fraction of spins 5/2 : $f_{5/2}$ is reported in Table S1. Interestingly, the highest $f_{5/2}$ ($\approx$ 90-87%) is found for A1-3 which contains a larger vesicle concentration.

The presence of a high spin state can be associated with long range intermolecular associations, such as found in vesicles, and low spin state (S=1/2) to Fe sites interacting with water, as expected at the edges of membrane fragments, or in free non-aggregated monomers. Spin crossover (SCO) of a complex compound in the bulk solid state is generally studied as a function of an external parameter, as temperature, pressure, light exposure.[43] Moreover, in nanomaterials, the size reduction can provide an additional tool to tune the SCO.[44] In the liquid state, it has been shown that a hysteretic spin transition can be induced in a solution assembly of a Fe^{3+} amphiphilic complex.[45,46] Here, the different spin states result from the presence or absence of molecular auto-assembly in water, depending on the surfactant concentrations. When involved in vesicles, the $FeCl_3Br^-$ anions are less exposed to water than non self-assembled monomers, [28] for which hydrogen bonding with the anion is allowed, and may induce a reduction of the molecular volume and a low spin state below the freezing temperature.

To support this statement, magnetic measurements have been performed with pure DATF and AOT$_3$F for a concentration (1.47 mM and 0.50 mM respectively) below the CMC (13.6 mM and 0.73 mM respectively) where dominating monomers are expected. Results are reported in figure S4 and S5. For both surfactants, the high spin concentration is close to 30-40 %, which assesses the attribution of spin ½ to monomers.
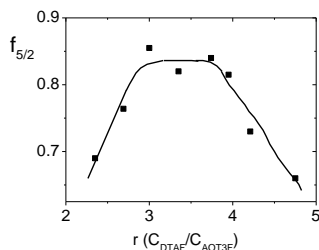
Figure 5: High spin fraction $f_{5/2}$ and θ as a function of the ratio "r" of DTAF and AOT$_3$F concentrations, the total surfactants concentration has been kept constant and equal to 5.4mM.

To investigate the distribution of surfactants in vesicles, magnetic measurements have been also performed as a function of surfactants ratio r, for a constant total surfactant concentration (equal to the one of A3). The fraction of high spin $f_{5/2}$, plotted in figure 5, presents a smooth maximum for r in between 3 and 4 and decreases below r ≈ 3 and above r ≈ 4. The decrease of $f_{5/2}$ above r ≈ 4 corroborates the results obtained for A and B solutions: in this ratio range, the vesicles concentration is limited by the AOT$_3$F concentration, and the additional proportion of DTAF is not involved in vesicles but is lost as monomers (or low spins) in the solution, or as micelles for higher DTAF excess. Below r ≈ 3, one could expect that the vesicles concentration is limited by the DTAF concentration, and then monomers of AOT$_3$F provide a low spin signal. This figure shows that despite vesicles can exist in a wide range of surfactant concentrations ratio, the ratio range indeed involved in the vesicles appears quite narrow, between roughly 3 and 4 DTAF molecules per AOT$_3$F molecule. As a result, vesicles of DTAF/AOT$_3$F result from an ordered molecular arrangement.

In conclusion, we show that the self-assembly of surfactants can be investigated through the spin state of the metallic centers. Moreover, with this tool, one can assess the critical vesicle concentration, and the partitioning of surfactants between bilayers and free in solution. This key property of vesicle systems cannot be addressed with techniques previously employed, therefore, the approach described here is unique and is expected to provide new insight into vesicle self-assembly.
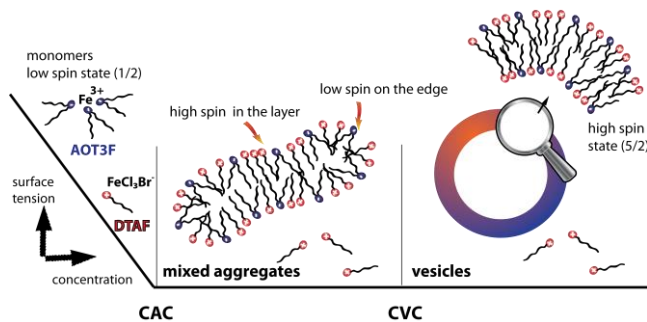

Figure 6. Schematic representation showing the spin crossover of self-assembled MagSurfs: low spin in monomers, low spin and high spin in bilayers and high spin in vesicles.

ASSOCIATED CONTENT

Supporting Information

Details on the synthesis and self-assembly characterization (Cryo-TEM, -STEM, DLS, NTA, SANS, surface tension and magnetic measurements) of surfactants are described in supporting information. This material is available free of charge via the Internet at http://pubs.acs.org.

AUTHOR INFORMATION

Corresponding Author

E-mail: andreea.pasc@univ-lorraine.fr, Tel: + 33 3 83 68 46 61; christine.bellouard@univ-lorraine.fr, Tel: +33 3 83 68 48 23.

Notes

The authors declare no competing financial interest.

REFERENCES

(1)   Kumar, G. P.; Rajeshwarrao, P. *Acta Pharm. Sin. B* **2011**, *1*, 208.
(2)   Sinico, C.; Fadda, A. M; *Expert Opin. Drug Deliv*. **2009**, *6*, 813.
(3)   Yuk, S. H.; Oh, K. S.; Koo, H.; Jeon, H.; Kim, K.; Kwon, I. C. *Biomaterials* **2011**, *32*, 7924.
(4)   Brinkhuis, R. P.; Rutjes, F. P. J. T.; van Hest, J. C. M. *Polym. Chem.* **2011**, *2*, 1449.
(5)   Debecker, D. P.; Faure, C.; Meyre, M.-E.; Derré, A.; Gaigneaux, E. M. *Small* **2008**, *4*, 1806.
(6)   Watanabe, K.; Takizawa, S.-Y.; Murata, S. *Chem. Lett*. **2011**, *40*, 345.
(7)   Adamala, K.; Szostak, J. W. *Nat Chem* .**2013**, *5*, 495.
(8)   Al Bawab, A.; Heldt, N.; Li, Y. *J. Dispersion Sci. Technol.* **2005**, *26*, 251.
(9)   Walde, P. *Bioessay s***2010**, *32*, 296.
(10)   Zhou, C.; Cheng, X.; Yan, Y.; Wang, J.; Huang, J. *Langmuir* **2014**, *30*, 3381.
(11)   Du, J.; Tang, Y.; Lewis, A. L.; Armes, S. P. *J. Am. Chem. Soc.* **2005**, *127*, 17982.
(12)   Wang, H.; Xu, F.; Wang, Y.; Liu, X.; Jin, Q.; Ji, J. *Polym. Chem*. **2013**, *4*, 3012.
(13)   Ren, T.-B.; Feng, Y.; Zhang, Z.-H.; Li, L.; Li, Y.-Y. *Soft Matter* **2011**, *7*, 2329.
(14)   Li, Q.; Chen, X.; Jing, B.; Zhao, Y.; Ma, F. *Colloids Surf., A* **2010**, *355*, 146.
(15)   Lecommandoux, S.; Sandre, O.; Chécot, F.; Rodriguez-Hernandez, J.; Perzynski, R. *Adv. Mater.* **2005**, *17*, 712.
(16)   Beaune, G.; Dubertret, B.; Clément, O.; Vayssettes, C.; Cabuil, V.; Ménager, C. *Angew. Chem. Int. Ed*. **2007**, *46*, 5421.
(17)   Ye, F.; Barrefelt, Å.; Asem, H.; Abedi-Valugerdi, M.; El-Serafi, I.; Saghafian, M.; Abu-Salah, K.; Alrokayan, S.; Muhammed, M.; Hassan, M. *Biomaterials* **2014**, *35*, 3885.
(18)   Sanson, C.; Diou, O.; Thévenot, J.; Ibarboure, E.; Soum, A.; Brûlet, A.; Miraux, S.; Thiaudière, E.; Tan, S.; Brisson, A. Dupuis, V.; Sandre, O.; Lecommandoux, S. *ACS Nano* **2011**, *5*, 1122.
(19)   Niu, D.; Wang, X.; Li, Y.; Zheng, Y.; Li, F.; Chen, H.; Gu, J.; Zhao, W.; Shi, J. *Adv. Mater.* **2013**, *25*, 2686.

(20)   Martina M-S.; Fortin J-P.; Ménager C.; Clément O.; Baratt G. ; Grabielle-Mademont C. ; Gazeau F. ; Cabuil V. ; Lesieur S. *J. Am. Chem. Soc.* **2005**, *127*, 10676.

(21)   Béalle, G.; Di Corato R.;Kolosnjaj-Tabi J. ; Dupuis V. ; Clément O. ; Gazeau F. ; Wilhem C. ; Ménager C. *Langmuir* **2012**, *28*, 11838.

(22)   Yang, X.; Pilla, S.; Grailer, J. J.; Steeber, D. A.; Gong, S.; Chen, Y.; Chen, G. *J. Mater. Chem.* **2009**, *19*, 5812.

(23)   Yang, X.; Grailer, J. J.; Rowland, I. J.; Javadi, A.; Hurley, S. A.; Matson, V. Z.; Steeber, D. A.; Gong, S. *ACS Nano* **2010**, *4*, 6805.

(24)   Arosio, P.; Thévenot, J.; Orlando, T.; Orsini, F.; Corti, M.; Mariani, M.; Bordonali, L.; Innocenti, C.; Sangregorio, C.; Oliveira, H.; Lecommandoux, S.; Lascialfari, A.; Sandre, O. *J. Mater. Chem. B* **2013**, *1*, 5317.

(25)   Zhou, J.; Chen, M.; Diao, G. *ACS Appl. Mater. Interfaces* **2014**, *6*, 18538.

(26)   Meyre, M.-E.; Clérac, R.; Mornet, S.; Duguet, E.; Dole, F.; Nallet, F.; Lambert, O.; Trépout, S.; Faure, C. *Phys. Chem. Chem. Phys.* **2010**, *12*, 12794.

(27)   Krack, M.; Hohenberg, H.; Kornowsli, A.; Lindner P.; Weller H.; Förster, S. *J. Am. Chem. Soc.* **2008**, *130*, 7315.

(28)   Brown, P.; Bushmelev, A.; Butts, C. P.; Cheng, J.; Eastoe, J.; Grillo, I.; Heenan, R. K.; Schmidt, A. M. *Angew. Chem. Int. Ed.* **2012**, *51*, 2414.

(29)   Brown, P.; Bushmelev, A.; Butts, C. P.; Eloi, J.-C.; Grillo, I.; Baker, P. J.; Schmidt, A. M.; Eastoe, J. *Langmuir* **2013**, *29*, 3246.

(30)   Brown, P.; Butts, C. P.; Eastoe, J.; Glatzel, S.; Grillo, I.; Hall, S. H.; Rogers, S.; Trickett, K. *Soft Matter* **2012**, *8*, 11609.

(31)   Kim, S.; Durand, P.; Roques-Carmes, T.; Eastoe, J.; Pasc, A. *Langmuir* **2015**, *31*, 1842.

(32)   Smith, G. N.; Eastoe, J. *J. Colloid Interface Sci.* **2014**, *426*, 252.

(33)   Brown, P.; Khan, A. M.; Armstrong, J. P. K.; Perriman, A. W.; Butts, C. P.; Eastoe, J. *Adv. Mater.* **2012**, *24*, 6244.

(34)   Kim, S. Bellouard, C.; Pasc, A.; Lamouroux, E.; Blin, J.-L.; Carteret, C.; Fort, Y.; Emo, M.; Durand, P.; Stébé, M.-J. *J. Mater. Chem. C* **2013**, *1*, 6930.

(35)   Michini Y. ; Carrière D. ; Mariet C. ; Moskura M. ; Berthault P. ; Belloni L. ; Zemb T. *Langmuir* **2009**, *25*, 698.

(36)   Béalle G. ; Jestin J. ; Carrière D. *Soft matter* **2011**, *7*, 1084.

(37)   Noirjean C. ; Testard F. ; Jestin J. ; Taché O. ;Dejugnat C. ; Carriere D. *Soft matter* **2014**, *10*, 5928.

(38)   Lin, C.; Zhao, J.; Jiang, R. *Chem. Phys. Lett.* **2008**, *464*, 77.

(39)   Hubbard, F. P.; Santonicola, G.; Kaler, E. W.; Abbott, N. L. *Langmuir* **2005**, *21*, 6131.

(40)   http://www.sasview.org/index.html.

(41)   Shioi, A.; Hatton, T. A. *Langmuir* **2002**, *18*, 7341.

(42)   O'Connor, A. J.; Hatton, T. A.; Bose, A. *Langmuir* **1997**, *13*, 6931.

(43)   Brooker S. *Chem. Soc. Rev.* **2015**, *44*, 2880.

(44)   Salmon L. ; Molnar G. ; Zitouni D.; Quintero C. ; Bergaud C. ; Micheau J.-P. ; Bousseksou A. *J. Mater. Chem.* **2010**, *20*, 5499.

(45)   Gaspar A.B.; Seredyuk M. *Coordination Chemistry Reviews* **2014**, *268*, 41.

(46)   Gandolfi C.; Morgan G.G.; Albrecht M. *Dalton Trans.* **2012**, *41*, 3726.
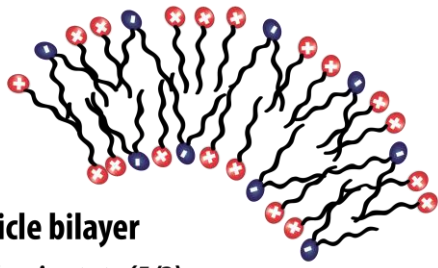
vesicle bilayer

high spin state (5/2)

monomers

low spin state (1/2)